Kinetic Chain Lengths in Highly Cross-Linked Networks Formed by the Photoinitiated Polymerization of Divinyl Monomers: A Gel Permeation Chromatography Investigation

ARTICLE *in* BIOMACROMOLECULES · JANUARY 2003

Impact Factor: 5.75 · DOI: 10.1021/bm025677o · Source: PubMed

3 AUTHORS, INCLUDING:

Tara M Lovestead
National Institute of Standards and Technolo…
41 PUBLICATIONS **855** CITATIONS
SEE PROFILE

Kristi Anseth
University of Colorado Boulder
356 PUBLICATIONS **20,367** CITATIONS
SEE PROFILE

Article

Kinetic Chain Lengths in Highly Cross-Linked Networks Formed by the Photoinitiated Polymerization of Divinyl Monomers: A Gel Permeation Chromatography Investigation

Jason A. Burdick, Tara M. Lovestead, and Kristi S. Anseth

Biomacromolecules, **2003**, 4 (1), 149-156• DOI: 10.1021/bm025677o • Publication Date (Web): 14 December 2002

Kinetic Chain Lengths in Highly Cross-Linked Networks Formed by the Photoinitiated Polymerization of Divinyl Monomers: A Gel Permeation Chromatography Investigation

Jason A. Burdick,† Tara M. Lovestead,† and Kristi S. Anseth*,†,‡

Department of Chemical Engineering and Howard Hughes Medical Institute, University of Colorado, Boulder, Colorado 80309-0424

Received September 13, 2002; Revised Manuscript Received November 14, 2002

Highly cross-linked networks formed by the photoinitiated polymerization of multifunctional monomers are finding application in the field of biomaterials because of their chemical versatility, reaction control, and ability to polymerize under physiological conditions. Typically, degradation is introduced into these networks via the cross-links and leads to the release of nondegradable but water-soluble kinetic chains formed during the chain polymerization process. In this study, gel permeation chromatography (GPC) was used to characterize kinetic chain length distributions in highly cross-linked systems that are being developed for orthopedic applications. By polymerizing divinyl monomers to various conversions and subsequently degrading them, we investigated the aspects of network structural evolution related to kinetic chain formation. In general, the average kinetic chain length increased with conversion until the onset of autodeceleration, when the kinetic chains decreased in length as the propagation reaction became diffusion-controlled. The distribution of kinetic chains also changed when different initiation conditions (i.e., initiator concentration and incident light intensity) were used, and a decrease in the kinetic chain lengths was observed at higher initiation rates. Finally, kinetic chain lengths were examined as a function of depth in thick samples polymerized with different light intensities and with a photobleaching initiator. Light attenuation through the sample led to different initiation rates as a function of depth and, consequently, spatial heterogeneity in the network structure as measured by the distributions of kinetic chains.

1. Introduction

Traditional applications of photopolymerized cross-linked networks include coatings, adhesives, and photolithography; however, the major benefits of photoinitiated polymerizations have prompted research into several additional areas, including biomaterials for dentistry and medicine. In general, photopolymerization occurs under ambient conditions without the use of a solvent, is compatible with a variety of chemistries, and provides spatial and temporal control to the initiation process.[1,2] Photopolymerization is used in the dental industry to form composites in situ as alternatives to mercury amalgam fillings. Dimethacrylate monomer solutions with suspended ceramic fillers are applied directly to the caries and polymerized with visible light to form a tooth-colored restoration. Composite resins are more aesthetic than traditional amalgams, are less toxic, and are easily applied to the dental defect.[3]

In situ photopolymerized and degradable biomaterials are also being developed for various tissue engineering and drug delivery applications.[4,5] For instance, highly cross-linked networks are being developed for tissue engineering scaffolds in orthopedics[6,7] and microparticles for drug delivery,[8] whereas loosely cross-linked hydrogel networks are being used for cell encapsulation,[9,10] growth factor delivery vehicles for tissue engineering,[11,12] and tissue adhesives.[13] Photopolymerization is an attractive technique to form biomaterials because polymerization is possible under physiological conditions (i.e., at body temperature and in the presence of biological fluids).

From a clinical perspective, highly cross-linked networks formed in vivo via a photoinitiated polymerization exhibit numerous benefits. First, filling a defect with an injectable or moldable reactive monomer solution that is polymerized intraoperatively eliminates the need for ex vivo fabrication of complex materials that must be subsequently implanted in the body. For example, dimethacrylate monomers were reacted in rat tibia defects, and no visible necrosis resulted from in situ photopolymerization, and good filling of the defects was observed, especially compared to control implants.[4] However, a major concern when in vivo cross-linking biomaterial networks is controlling the polymerization so that sufficient conversions are reached on suitable time scales. To address this concern, temporal control of photoinitiation can be used to minimize temperature rises during polymerization while maintaining high conversions with depth. In a previous study,[14] temperature rises and conversions with depth were analyzed for a variety of initiation conditions. The major conclusions from the study were that the polymerization of thick implants is very controllable and that a

* To whom correspondence should be addressed.
† Department of Chemical Engineering.
‡ Howard Hughes Medical Institute.

10.1021/bm025677o CCC: $25.00
Published on Web 12/14/2002

photobleaching or dual initiating system may be beneficial in initiating the polymerization.

Assessing the implications of the reaction conditions on the network structure is important when using these approaches to control the polymerization behavior of multifunctional monomers. Typically, degradation is incorporated into these networks through labile bonds in the cross-links. Thus, upon degradation, the release of kinetic chains formed from the photoinitiated chain polymerization will depend strongly on their length and distribution of molecular weights, which are inherently dependent on factors such as the rate of initiation and polymerization kinetics. Thus, experimental techniques to characterize the kinetic chains in cross-linked networks are important.

While linear polymers are widely characterized through techniques such as gel permeation chromatography (GPC) and nuclear magnetic resonance (NMR), cross-linked networks pose problems because they are inherently insoluble, which limits the application of many standard analytical techniques. Radical chain polymerizations of multifunctional monomers are extremely complex, and the polymerization rate and evolving network structure are influenced by changes in the initiation rate, macromer size and flexibility, and solvent concentration.[15,16] The polymerization is further complicated by diffusion limitations that are dependent on network conversion. By studying monomer systems that react to form degradable cross-linked networks and subsequently isolating and analyzing the kinetic chains with techniques used for analysis of linear systems, researchers are now able to further investigate cross-linked networks that were previously difficult to understand. For example, Burkoth and Anseth[17] utilized matrix-assisted laser desorption/ionization time-of-flight (MALDI-TOF) mass spectrometry to investigate kinetic chain distributions in degradable cross-linked networks. The study concluded that the number-average degree of polymerization decreased with increased double-bond conversion and at faster initiation rates and the distribution of the analyzed chains varied significantly from the Flory most probable distribution. Although not completely understood, the molecular weight of degradation products has implications on both the biocompatibility of these materials and various physical properties. For instance, investigators have shown that water-soluble polymers that exceed a critical molecular weight can accumulate in the body's circulatory system.[18]

The overall objective of this study was to utilize size-exclusion chromatography (i.e., GPC) to investigate kinetic chain length distributions formed during the photoinitiated polymerization of a low molecular weight divinyl monomer, specifically one that reacts to form a polyanhydride network that is being developed as an in-situ-forming orthopedic biomaterial. First, the kinetic chain molecular weight evolution during polymerization was investigated by polymerizing the monomer to various conversions, shuttering the initiating light source, and analyzing the kinetic chains in the degradation products. Next, the dependence of polymerization initiation conditions (i.e., light intensity and photoinitiator concentration) on kinetic chain lengths was investigated. Finally, because numerous applications require the formation of thick, three-dimensional implants, changes in the network structure with depth were studied by examining the kinetic chains in thick materials fabricated under various initiation conditions.

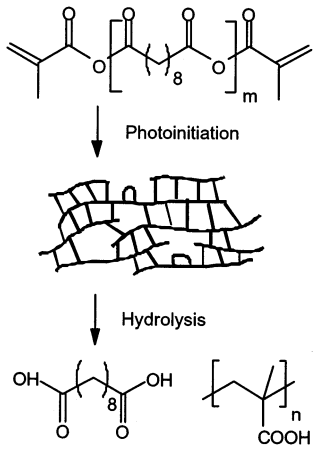

Figure 1. Chemical structure of methacrylated sebacic acid (MSA). MSA forms a highly cross-linked network via a photoinitiated chain polymerization and degrades upon hydrolysis of the labile anhydride linkages in the cross-links into sebacic acid and poly(methacrylic acid) (PMAA) kinetic chains.

2. Experimental Section

2.1. Network Synthesis and Degradation. Dimethacrylated sebacic acid (MSA, Figure 1) was synthesized as described in detail elsewhere.[7] Photoinitiators used in this study included 2,2-dimethoxy-2-phenyl acetophenone (DMPA, Ciba-Geigy) and benzoin ethyl ether (BEE). DMPA is a commonly used ultraviolet initiator, whereas BEE is known to photobleach upon exposure to ultraviolet light,[14] so the initiator fragments absorb light at a different wavelength than the initiating light source. All materials were used as received from Aldrich unless noted otherwise.

Photoinitiators at a concentration of 0.1 wt % were dissolved in MSA at ~60 °C. Samples were polymerized at room temperature between glass slides with a spacing of 0.5 mm using a Novacure (EFOS) light source with a 365 nm filter and light intensities ranging from 2.5 to 100 mW/cm^2 for 5 min. For characterization of network structural evolution in thick samples, MSA was polymerized for 15 min in a Teflon mold (diameter = 5 mm, height = 10 mm) covered with a glass slide and cut into thirds (top, 0.0−0.33 cm; middle, 0.33−0.67 cm; and bottom, 0.67−1.0 cm). Samples were degraded (37 °C on an orbital shaker) completely in deionized water, dialyzed to remove salts, frozen at −80 °C, and lyophilized for storage before GPC analysis. All sample conditions were performed at least in duplicate.

2.2. Reaction Characterization. The polymerization behavior of MSA with time was characterized using differential scanning calorimetry (DSC, Perkin-Elmer DSC7). Isothermal conditions were maintained at room temperature with an external chiller (NESLAB RTE-111) attached to the DSC. The MSA/initiator sample (~5 mg) was placed in the bottom of an aluminum DSC pan, and the heat flux was monitored during irradiation as described above. This sample size produced only a thin film (thickness < 0.2 mm) on the

bottom of the DSC pan. The rate of polymerization (R_p) was obtained using a ΔH_{rxn} of −13.1 kcal/mol,[19] and the conversion was obtained by integrating the R_p versus polymerization time curve.

2.3. GPC Analysis of Kinetic Chains. Lyophilized samples were dissolved in 0.1 M sodium nitrate and filtered through a 0.45 μm syringe filter before manual injection into a Waters GPC system (1 mL/min, 35 °C) equipped with Polymer Standard Services Suprema columns (guard, linear, 30, 100, and 1000 Å) and a Waters refractive index detector (model 2410). The molecular weights and polydispersities of the degradation products were calibrated using poly(methacrylic acid) (PMAA) standards with an internal standard of ethylene glycol. The greater the sample volume required to elute the sample was, the smaller the kinetic chain lengths were because of increased time spent in the porous packing material (i.e., 1 mL is equivalent to 1 min on the column). Duplicate samples were run for each reaction condition.

3. Results and Discussion

Kinetic chain distributions in highly cross-linked networks formed by chain polymerization of divinyl monomers were determined by degrading networks formed under various initiation conditions and analyzing the degradation products with GPC. In addition, thick samples were prepared, and the degradation products were analyzed as a function of depth. The MSA-based networks degrade by a surface erosion mechanism exclusively into sebacic acid and PMAA kinetic chains (Figure 1). By analyzing the length of the kinetic chains through GPC, information about the network evolution and structure can be obtained. In typical nondegradable networks, this analysis is complicated by the inability to isolate kinetic chains from the networks. In degradable biomaterials, information regarding the kinetic chains is important in terms of the heterogeneity in structure with sample depth and in the release and biocompatibility of degradation products.

3.1. General Polymerization Behavior. To help in interpretation and discussion of the kinetic chain lengths determined experimentally with GPC, several of the governing equations that are useful in characterization of photoinitiated polymerizations are reviewed. First, the initiation rate (R_i) for the photoinitiation process is calculated from the following equation assuming thin films with uniform light intensity:[20]

$$R_i = 2\Phi f I = 2\Phi f\left(\frac{2.303\epsilon I_0 \lambda c_I}{N_{Av} hc}\right) \tag{1}$$

Here, Φ is the number of radicals produced per light photon absorbed (assumed equal to 1), f is the photoinitiator efficiency (assumed equal to 1 for R_{i0} calculations), I is the molar quantity of light absorbed, ϵ is the molar absorptivity of the initiator (150 L/(mol cm) for DMPA at $\lambda = 365$ nm), I_0 is the incident light intensity, c_I is the initiator concentration, N_{Av} is Avogadro's number, h is Planck's constant, and c is the velocity of light. The two parameters that are easy to change to alter R_i are the initiator concentration and the initiating light intensity. The initiator efficiency also changes with conversion in the sample as the network becomes diffusion-limited. For biological applications, it is necessary to keep the light intensity low enough and λ high enough to prevent necrosis of tissue surrounding the polymerizing implant, and as will be discussed in detail later, the initiator concentration can dramatically affect light attenuation through thick samples.

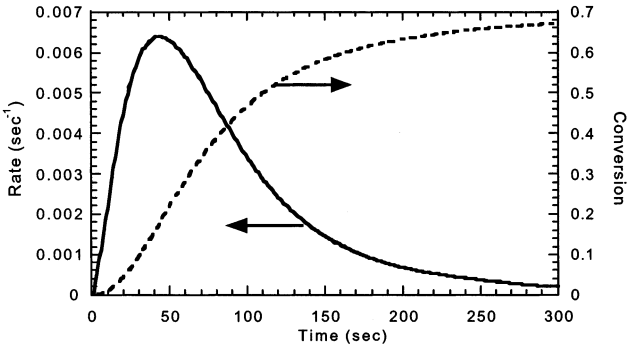

Figure 2. R_p and conversion versus time for the polymerization of MSA initiated with 2.5 mW/cm^2 and 0.1 wt % DMPA determined with DSC.

The polymerization rate (R_p) is given by the following equation:[20]

$$R_p = -\frac{d[M]}{dt} = k_p[M][R\bullet] \tag{2}$$

where [M] is the double bond concentration, t is the polymerization time, k_p is the free-volume-dependent propagation kinetic constant,[21−26] and [R•] is the radical concentration. The radical concentration is calculated by the following equation:

$$\frac{d[R\bullet]}{dt} = R_i - R_t \tag{3}$$

where R_t is the bimolecular termination rate ($R_t = 2k_t[R\bullet]^2$). Here, k_t is the free-volume-dependent termination kinetic constant.[21,23−26] These equations combine to reveal a polymerization rate dependence on the changing kinetic constants, double bond concentration, and initiation rate. An additional factor that can complicate the polymerization behavior is the consumption of the photoinitiator with polymerization, given by the following equation:

$$c_I = c_{I0} \exp\left(\frac{-2.303\epsilon I_0 \lambda}{N_{Av} hc} t\right) \tag{4}$$

where c_{I0} is the initial initiator concentration. This exponential decay in initiator concentration can change R_i and, consequently, R_p throughout the polymerization.

A representative plot of R_p versus polymerization time for MSA initiated with 2.5 mW/cm^2 and 0.1 wt % DMPA as determined using DSC is shown in Figure 2. This rate curve is typical for radical chain polymerizations of multifunctional monomers that are diffusion-controlled at very early polymerization times. Instead of R_p decreasing because of decreased monomer and initiator consumption, as one might expect, R_p increases throughout the initial polymerization. This

counterintuitive increased polymerization rate is referred to as autoacceleration and is caused by an almost instantaneous build up of high molecular weight polymer chains and an early onset of gelation. This regime is characterized by a rapid increase in viscosity due to the high molecular weight polymer chains and a subsequent decrease in mobility of the growing radical chains. At low conversion, free volume theory dictates that the termination reaction between two growing radical chains is mobility restricted while the propagation reaction is unrestricted because monomer is still readily mobile. Examination of eq 3 reveals that the increase in [R•], which is a result of the decrease in bimolecular termination, induces an overall increase in polymerization rate.

As the polymerization reaction proceeds, R_p is observed to decrease with the onset of autodeceleration, where propagation becomes diffusion-controlled. This regime in photoinitiated radical polymerizations is characterized by an even greater viscosity increase accompanied by a significant decrease in the mobility of all reactive molecules. Both propagation and termination kinetics are affected and observed to decrease significantly, and consequently, R_p is observed to decrease for the remainder of the polymerization.

For the photopolymerization of thick samples, light attenuation through the sample can also dramatically change the initiation rate spatially. Light attenuation as a function of sample depth is given by the Beer−Lambert law:

$$I = I_0 \exp(-2.303\epsilon c_I z) \tag{5}$$

where I is the light intensity at depth z. This equation assumes that there is no diffraction or scattering of the initiating light throughout the sample, which complicates the analysis even further. The exponential decrease in light intensity can significantly change R_i throughout the sample, depending on the initiator concentration and light intensity.

Due to the complexity in the polymerization behavior, the average kinetic chain length ($\bar{\nu}$) evolution is not well understood. To aid in our understanding of kinetic chain lengths, the instantaneous, that is, average, kinetic chain length for bimolecular termination in the absence of chain transfer was predicted (eq 6).

$$\bar{\nu} = \frac{R_p}{R_t} = \frac{k_p[M]}{2k_t[R\bullet]} \tag{6}$$

Figure 3 depicts $\bar{\nu}$ as a function of conversion as predicted by a free volume model that incorporates eqs 1−4 and 6 for a typical multifunctional photopolymerization. The model incorporates material and physical properties for diethylene glycol dimethacrylate (DEGDMA), a multifunctional monomer that has been extensively characterized through both modeling and experimentation[25−28] and is similar in chemistry and functionality to MSA. Figure 3 reveals that the instantaneous kinetic chain length predicted is greatly dependent on the same mobility restrictions that affect polymerization rate. Specifically, the kinetic chains increase throughout autoacceleration and decrease throughout autodeceleration. Equation 6 can also be related to the instantaneous number-average degree of polymerization for termination by disproportionation (which is proportional to the number-average molecular weight), in contrast to the cumulative molecular weight distribution of chains, born throughout the entire polymerization, given by GPC.[20] As discussed above, the kinetic constants, light intensity, and initiator concentration can dramatically change the kinetic chain lengths. The dynamic behavior of these properties leads to a complex polymerization mechanism and a correspondingly complex network structure.

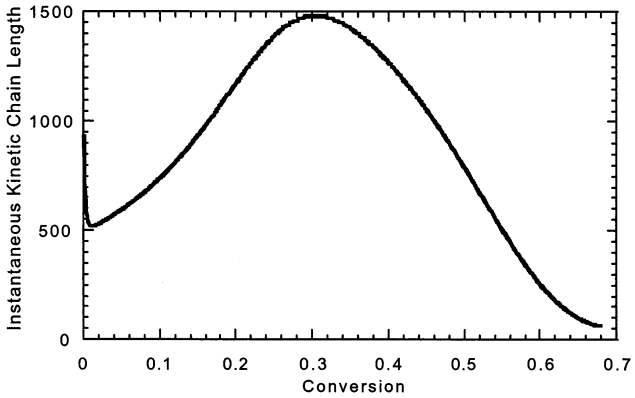

Figure 3. Average kinetic chain length versus conversion for the free volume model simulation of a thin film photopolymerization of DEGDMA at 2.5 mW/cm^2 with 0.1 wt % DMPA.

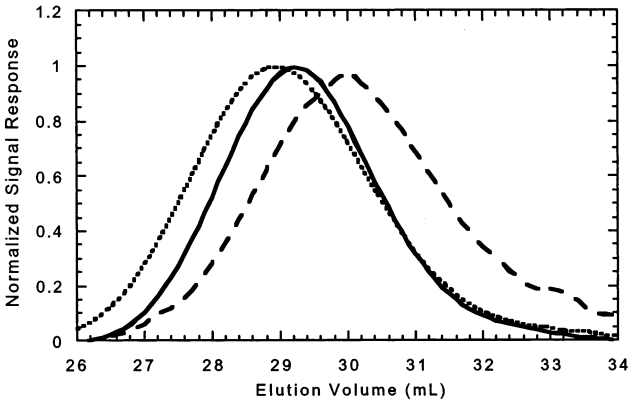

Figure 4. Kinetic chain lengths for the polymerization of MSA with 2.5 mW/cm^2 and 0.1 wt % DMPA for 20 (dashed line), 60 (dotted line), and 180 s (solid line) determined with GPC.

This discussion of the photopolymerization of thick materials illustrates the overall complexity of photoinitiated chain polymerizations of multifunctional monomers and the difficulty in accurately determining structural properties such as kinetic chain lengths, in thick highly cross-linked polymers. For this reason, experimental techniques to measure actual chain lengths and changes in kinetic chains with initiation conditions and spatial locations in a polymerizing sample are necessary to further understand these materials. The remainder of this paper will focus on experimental measurements of kinetic chains using GPC.

3.2. Network Formation. The kinetic chain length distribution at specific time points (20, 60, and 180 s) was determined (Figure 4) for the same initiation conditions as observed in Figure 2 (I_0 = 2.5 mW/cm^2 with 0.1 wt % DMPA). Quantified results are listed in Table 1. The corresponding percent conversions (X), determined by integrating the rate of polymerization versus time plot, were 4%, 28%, and 62%. After 20 s of polymerization, a kinetic chain

Table 1. Kinetic Chain Length Distributions during the Polymerization of MSA with 0.1 wt % DMPA and 2.5 mW/cm^2 Ultraviolet Light ($R_i = 2.06 \times 10^{-5}$ mol/(L s))

polymerization time (s)	conversion (%)	$\bar{M}_n$ (kDa)	$\bar{n}_n$	Q
20	4.3	130	1600	2.8
60	28.2	190	2200	2.6
180	61.7	180	2000	1.7

length distribution comprised of some of the smallest chains ($\bar{M}_n = 130$ kDa) was observed. While the reacting system was autoaccelerating, the cumulative average kinetic chain length increased from 130 to 190 kDa, and this increase was attributed to the kinetic chain length dependence on k_t and [R•] as shown in eq 6. Specifically, k_t is mobility-restricted, and thus, [R•] increases during autoacceleration, which leads to an increase in $\bar{\nu}$ for chains born during this region of the polymerization. While this equation supports the general trends that are observed, it is important to point out that there are many assumptions inherent in this equation, such as bimolecular termination and chain-length-independent termination. Additionally, the equation only determines the instantaneous kinetic chain length in contrast to the GPC, which measures the integrated kinetic chains born at all times.

The long autodeceleration period produced a large population of shorter kinetic chains, denoted by a shift in elution volume toward higher volumes (i.e., $\bar{M}_n = 180$ kDa after 180 s). This decrease in kinetic chain lengths was attributed to decreases in the propagation kinetic constant at higher conversions. The final kinetic chain length distribution was determined after 300 s of polymerization, corresponding to 67% conversion and a polymerization rate near zero. This corresponded to a slight increase in kinetic chain lengths and a shifting of the elution volume toward lower volumes. This region of polymerization is the least understood because of persistent radicals, incomplete conversion, and a highly cross-linked immobile network. At this high conversion, few of the fundamental polymerization equations are valid. The increased polymer molecular weight could be attributed to increased chain transfer to polymer at the higher conversions. In summary, GPC results show that the kinetic chain lengths vary in a complex way with network conversion and the polydispersity (Q) of the kinetic chains remained relatively low (i.e., ~1.7−2.8) and constant throughout the polymerization. However, it is necessary to investigate techniques that can be used to control the length and distribution of kinetic chains when designing in-situ-forming biomaterials.

3.3. Influence of Initiation Conditions. As seen in eqs 1 and 2, changes in the initiation conditions during multifunctional monomer photopolymerization lead to changes in R_i and, consequently, changes in R_p. Thus, changes in either the initiating light intensity or initiator concentration could be an easy method to control kinetic chain lengths. From the DSC results, shown in Figure 5a, there are dramatically different R_p versus polymerization time profiles when the initiator concentration (0.1−1.0 wt %) and the initiating light intensity (2.5−25 mW/cm^2) were altered. Although the general rate profile for all conditions was typical for multivinyl polymerizations, the time for complete polymerization and the magnitude and conversion at which the maximum polymerization rate occurs change with the initiation conditions. For instance, when 0.1 wt % DMPA is used for initiation, $R_{p,max}$ is ~0.02 s^{-1} with 25 mW/cm^2 ultraviolet light and only ~0.006 s^{-1} when 2.5 mW/cm^2 ultraviolet is used to initiate the polymerization, almost a 3-fold difference.

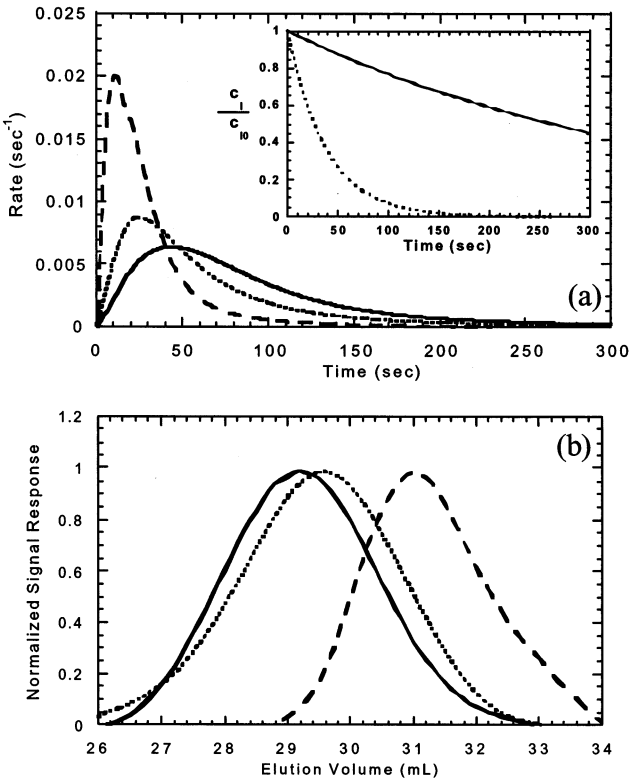

Figure 5. Influence of initiation conditions, 2.5 mW/cm^2 and 0.1 wt % DMPA (solid line), 2.5 mW/cm^2 and 1.0 wt % DMPA (dotted line), and 25 mW/cm^2 and 0.1 wt % (dashed line), on (a) R_p with polymerization time (inset shows fraction of initiator consumed during polymerization with either 2.5 (solid line) or 25 mW/cm^2 (dotted line)) and (b) kinetic chain lengths determined with GPC.

Table 2. Kinetic Chain Length Distributions of MSA Samples Polymerized with Various Initiation Conditions for 300 s

c_I (wt %)	I_0 (mW/cm^2)	R_{i0} (mol/(L s))	$\bar{M}_n$ (kDa)	$\bar{n}_n$	Q
1.0	2.5	2.1×10^{-4}	170	1900	2.2
0.1	2.5	2.1×10^{-5}	190	2200	1.8
0.1	25.0	2.1×10^{-4}	73	840	1.2

Interestingly, even though two of these initiation conditions were chosen because they had equal R_{i0} (Table 2), their R_p versus polymerization time profiles were dramatically different. This observation could be due to several factors including an increase in temperature with the higher light intensity due to absorption of the light by the sample or light attenuation in the sample with a high initiator concentration. Temperature increases can accelerate polymerizations, while light attenuation can decrease the incident light intensity and, consequently, R_i. However, neither of these factors was expected to play a significant role for samples polymerized in the DSC, which are polymerized as very thin films with a large heat sink to maintain isothermal conditions. An additional explanation for differences in the polymerization profiles with different initiation conditions is the consumption of initiator with polymerization time. For instance, when eq

Table 3. Approximate Percent Conversion during the Photoinitiated Polymerization of Thick Materials under Various Initiation Conditions[14]

initiation condition	top (0.0 cm)	middle (0.5 cm)	bottom (1.0 cm)
0.1 wt % DMPA, 25 mW/cm^2	92	79	16
0.1 wt % DMPA, 100 mW/cm^2	95	82	38
0.1 wt % BEE, 100 mW/cm^2	86	90	54

4 is used (i.e., species balance on the initiator) to calculate the fraction of initiator left after 300 s of polymerization, 0.046 (4.6% of initial concentration), 0.46 (46% of initial concentration), and 3.7×10^{-5} (<0.01% of initial concentration) wt % initiator remained for samples initiated with 0.1 wt % DMPA at 2.5 mW/cm^2, 1.0 wt % DMPA at 2.5 mW/cm^2, and 0.1 wt % DMPA at 25 mW/cm^2, respectively. The fraction of initiator consumed during polymerization is illustrated in Figure 5a (inset). Thus, even though R_p only depends on $R_i^{1/2}$ and $\bar{\nu}$ depends on $R_i^{-1/2}$, changes to R_i via the light intensity also alter the initiator rate consumption and further complicate the rate behavior and kinetic chain length evaluation.

The GPC results for samples polymerized with these various initiation conditions are shown in Figure 5b and quantified in Table 2. These results match expected trends for changes in initiation conditions. As the light intensity and initiator concentration were increased, the PMAA degradation products eluted at longer volumes, indicating that smaller kinetic chains were produced as R_i increased. For example, $\bar{M}_n$ for the kinetic chains decreased from 190 to 170 kDa when the initiator concentration was increased from 0.1 to 1.0 wt %. The increase in initiator concentration should increase R_i and, accordingly, decrease $\bar{\nu}$. Similarly, $\bar{M}_n$ for the kinetic chains decreased further to 73 kDa when the initiating light intensity was increased from 2.5 to 25 mW/cm^2. Because a greater number of radicals are formed with the increase in initiation rate, a decrease in kinetic chain length is expected because the probability of chain termination increases as well. Of further note, the initiating light intensity influenced the kinetic chain length more significantly than the initiator concentration, and simple analysis of R_{i0} was not sufficient to explain this complex dependence. However, the trend directly matches what was observed with the DSC results, indicating that R_p profiles could be a good indicator for the expected kinetic chain lengths for specific initiation conditions.

3.4. Influence of Sample Thickness. Because typical investigations of photopolymerization usually involve thin film applications such as photolithography and coatings, an investigation of thick network polymerization is essential when examining the potential of photopolymerization to form orthopedic biomaterials. Depending on the initiator concentration used, the light intensity can vary dramatically through different layers in the polymerizing biomaterial. From a previous study,[14] double bond conversions were determined at the sample surface and at depths of 0.5 and 1.0 cm and are listed in Table 3 for the initiation conditions used in the present study. The conversions change dramatically with light intensity, type of initiator, and depth in the samples and are representative of the heterogeneity that exists in thick samples polymerized with a photoinitiated free radical polymerization. Temperature rises and heat transfer in these samples both add to the complexity of understanding the polymerizations because the kinetic constants are functions of temperature.

Table 4. Kinetic Chain Lengths during the Photoinitiated Polymerization of Thick (1 cm) MSA Networks at the Top (0.0−0.33 cm), Middle (0.33−0.67 cm), and Bottom (0.67−1.0 cm) of the Samples

initiation condition	sample location	R_{i0} (mol/(L s))	$\bar{M}_n$ (kDa)	$\bar{n}_n$	Q
0.1 wt % DMPA, 25 mW/cm^2	top	2.1×10^{-4} to 1.3×10^{-4}	79	920	2.7
	middle	1.3×10^{-4} to 8.3×10^{-5}	270	3200	3.0
	bottom	8.3×10^{-5} to 5.3×10^{-5}	410	4800	5.9
0.1 wt % DMPA, 100 mW/cm^2	top	8.2×10^{-4} to 5.3×10^{-4}	58	670	1.6
	middle	5.3×10^{-4} to 3.3×10^{-4}	130	1500	2.7
	bottom	3.3×10^{-4} to 2.1×10^{-4}	330	3800	8.1
0.1 wt % BEE, 100 mW/cm^2	top	*a*	87	1000	1.8
	middle	*a*	140	1600	2.6
	bottom	*a*	270	3100	7.4

[a] Not determined.

Kinetic chain lengths for thick samples polymerized with various light intensities and initiators are listed in Table 4. Additionally, a plot of GPC results is shown in Figure 6a for samples initiated with 0.1 wt % DMPA and 25 mW/cm^2. In general, the kinetic chain lengths increased with sample depth. For example, $\bar{M}_n$ was equal to 79 kDa in the top section but increased to 270 kDa in the middle section and 410 kDa in the bottom section. A decrease in light intensity deeper into the sample led to a decrease in R_i and could explain the trends seen with the kinetic chains. There is also a trend of increasing polydispersity with depth in the sample.

The GPC results for thick samples polymerized with 100 mW/cm^2 ultraviolet light and 0.1 wt % of DMPA are shown in Figure 6b. The results follow similar trends to the sample polymerized with 25 mW/cm^2 with an increase in kinetic chain length with depth into the sample. With these initiation conditions, $\bar{M}_n$ increased from 58 kDa in the top section to 330 kDa in the bottom section for polymerizations with DMPA as the initiator. These chain lengths are shorter than the chain lengths at the same depths when the sample was polymerized with 25 mW/cm^2, corresponding to an increased R_i with higher light intensities. From eq 5, only ~6.5 mW/cm^2 of light reaches a depth of 1 cm when the sample is polymerized with 25 mW/cm^2, whereas ~25.9 mW/cm^2 light is transmitted to the same depth when the sample is initiated with 100 mW/cm^2. When a photobleaching initiator was used (BEE), $\bar{M}_n$ increased from 87 kDa in the top section to 270 kDa in the bottom section (Figure 6c). The smaller change in kinetic chain lengths throughout the sample with BEE compared to a sample polymerized with the same light intensity but using DMPA as the initiator could be due to the photobleaching nature of the initiator. A photobleaching

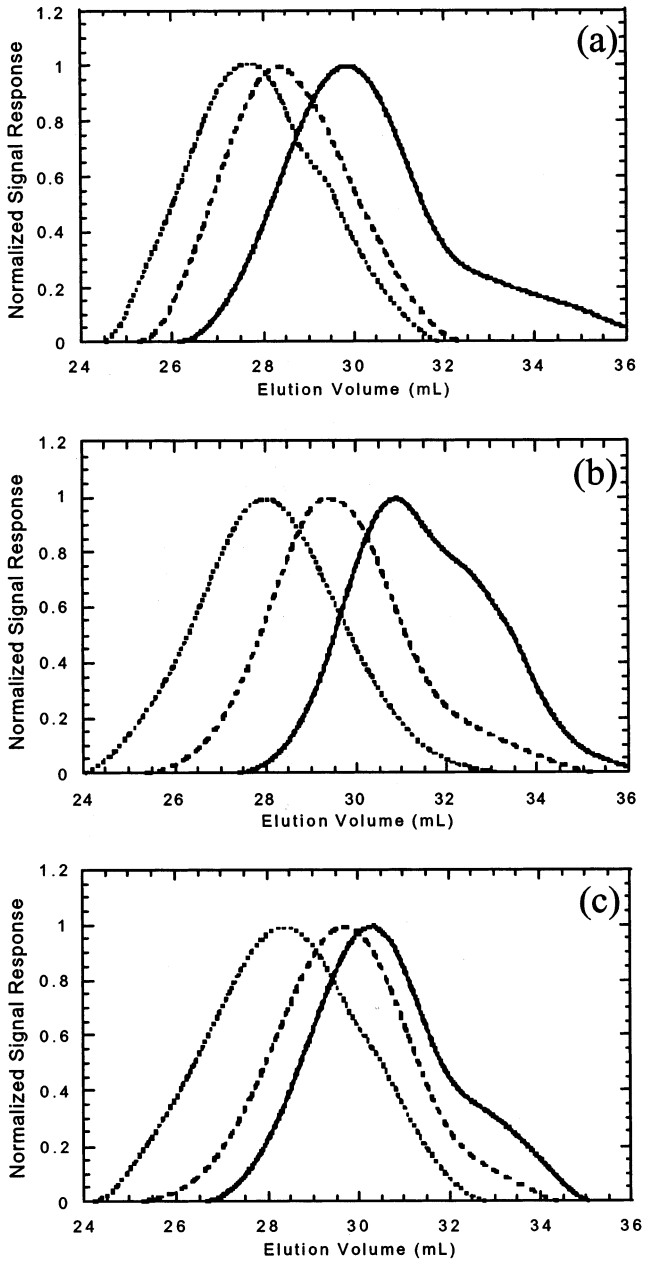

Figure 6. GPC profiles for the top (0−0.33 cm, solid line), middle (0.33−0.67 cm, dashed line), and bottom (0.67−1.0 cm, dotted line) of 1 cm thick samples initiated with (a) 25 mW/cm^2 ultraviolet light and 0.1 wt % DMPA, (b) 100 mW/cm^2 ultraviolet light and 0.1 wt % DMPA, and (c) 100 mW/cm^2 ultraviolet light and 0.1 wt % BEE.

initiator allows more light to penetrate to greater depths in the sample and led to higher conversions at a depth of 1 cm under these same conditions (Table 3). Because the initiating light (and therefore polymerization) is more uniform in the sample, the smaller change in the kinetic chain lengths throughout the sample might be expected.

4. Conclusions

GPC was used to characterize kinetic chain degradation products from highly cross-linked polyanhydride networks that are being developed as in-situ-forming biomaterials for orthopedic applications. Because of the chemistry of these networks, the PMAA kinetic chains are readily isolated from the low molecular weight degradation products. Free radical polymerizations of multifunctional monomers used to form these networks are highly complex because of changes in reactive species mobility, initiator consumption, and light intensity with polymerization time and depth. Kinetic chain length distributions were dependent on the double bond conversion and initiation rate. For thick samples, a general trend of increasing kinetic chain lengths with sample depth was observed and dependent on not only the initiating light intensity but also the type of initiator used.

References and Notes

(1) Decker, C. The use of UV irradiation in polymerization. *Polym. Int.* **1998**, *45*, 133−141.
(2) Narayanan, V.; Scranton, A. B. Photopolymerization of composites. *Trends Polym. Sci.* **1997**, *5*, 415−419.
(3) Anseth, K. S.; Newman, S. M.; Bowman, C. N. Polymeric dental composites: Properties and reaction behavior of multimethacrylate dental restorations. *Adv. Polym. Sci.* **1995**, *122*, 177−217.
(4) Anseth, K. S.; Burdick, J. A. New directions in photopolymerizable biomaterials. *MRS Bull.* **2002**, *27*, 130−136.
(5) Fisher, J. P.; Dean, D.; Engel, P. S.; Mikos, A. G. Photoinitiated polymerization of biomaterials. *Annu. Rev. Mater. Res.* **2001**, *31*, 171−181.
(6) Burdick, J. A.; Philpott, L. M.; Anseth, K. S. Synthesis and characterization of tetrafunctional lactic acid oligomers: A potential in situ forming degradable orthopaedic biomaterial. *J. Polym. Sci., Part A: Polym. Chem.* **2001**, *39*, 683−692.
(7) Anseth, K. S.; Shastri, V. R.; Langer, R. Photopolymerizable degradable polyanhydrides with osteocompatibility. *Nat. Biotechnol.* **1999**, *17*, 156−159.
(8) Owens, J. L.; Anseth, K. S.; Randolph, T. W. Compressed antisolvent precipitation and photopolymerization to form highly cross-linked polymer particles. *Macromolecules* **2002**, *35*, 4289−4296.
(9) West, J. L.; Hubbell, J. A. Polymeric biomaterials with degradation sites for proteases involved in cell migration. *Macromolecules* **1999**, *32*, 241−244.
(10) Bryant, S. J.; Anseth, K. S. The effects of scaffold thickness on tissue engineered cartilage in photocrosslinked poly(ethylene oxide) hydrogels, *Biomaterials* **2001**, *22*, 619−626.
(11) Anseth, K. S.; Metters, A. T.; Bryant, S. J.; Martens, P. J.; Elisseeff, J. H.; Bowman, C. N. In situ forming degradable networks and their application in tissue engineering and drug delivery. *J. Controlled Release* **2002**, *78*, 199−209.
(12) Burdick, J. A.; Mason, M. N.; Hinman, A. D.; Thorne, K.; Anseth, K. S. Sustained release of osteoinductive growth factors from degradable PEG hydrogels influences osteoblast differentiation and mineralization. *J. Controlled Release* **2002**, *83*, 53−63.
(13) Silverman, R. P.; Elisseeff, J.; Passaretti, D.; Huang, W.; Randolph, M. A.; Yaremchuck, M. J. Transdermal photopolymerized adhesive for seroma prevention. *Plast. Reconstr. Surg.* **1999**, *103*, 531−535.
(14) Burdick, J. A.; Peterson, A. J.; Anseth, K. S. Conversion and temperature profiles during the photoinitiated polymerization of thick orthopaedic biomaterials. *Biomaterials* **2001**, *22*, 1779−1786.
(15) Anseth, K. S.; Wang, C. M.; Bowman, C. N. Reaction behavior and kinetic constants from photopolymerizations of multi(meth)acrylate monomers. *Polymer* **1994**, *35*, 3242−3250.
(16) Elliot, J. E.; Anseth, J. W.; Bowman, C. N. Kinetic modeling of the effect of solvent concentration on primary cyclization during polymerization of multifunctional monomers. *Chem. Eng. Sci.* **2001**, *56*, 3173−3184.
(17) Burkoth, A. K.; Anseth, K. S. MALDI-TOF characterization of highly cross-linked, degradable polymer networks. *Macromolecules* **1999**, *32*, 1438−1444.
(18) Murakami, Y.; Tabata, Y.; Ikada, Y. Effect of the molecular weight of water-soluble polymers on accumulation at an inflammatory site following intravenous injection. *Drug Delivery* **1996**, *3*, 231−238.
(19) Leonard, J. Heats and entropies of polymerization, ceiling temperatures, equilibrium monomer concentrations, and polymerizability of heterocyclic compounds. In *Polymer Handbook*; Brandup, J.,

Immergut, E. H., Grulke, E. A., Eds.; John Wiley and Sons: New York, 1999; Section II, p 369.
(20) Odian, G. *Principles of polymerization*; John Wiley and Sons: New York, 1991.
(21) Bueche, F. *Physical Properties of Polymers*; Interscience: London, 1962.
(22) Soh, S. K.; Sundberg, D. C. Diffusion-controlled vinyl polymerization. III. free volume parameters and diffusion-controlled propagation. *J. Polym. Sci., Polym. Chem. Ed.* **1982**, *20*, 1331−1344.
(23) Martin, F. L.; Hamielec, A. E. High-conversion diffusion-controlled polymerization of styrene. I. *J. Appl. Polym. Sci.* **1982**, *27*, 489−505.
(24) Bowman, C. N.; Peppas, N. A. Coupling of kinetics and volume relaxation during polymerization of multiacrylates and multimethacrylates. *Macromolecules* **1991**, *24*, 1914−1920.
(25) Anseth, K. S.; Bowman, C. N. Reaction diffusion enhanced termination in polymerizations of multifunctional monomers. *Polym. React. Eng.* **1992**−**1993**, *4*, 499−520.
(26) Goodner, M. D.; Lee, H. R.; Bowman, C. N. Method for determining the kinetic parameters in diffusion-controlled free-radical homopolymerizations. *Ind. Eng. Chem. Res.* **1997**, *36*, 1247−1252.
(27) Lovestead, T. M.; Berchtold, K. A.; Bowman, C. N. Modeling the effects of chain length on the termination kinetics in multivinyl photopolymerizations. *Macromol. Theory Simul.* **2002**, *11*, 729−738.
(28) Berchtold, K. A.; Lovestead, T. M.; Bowman, C. N. Coupling chain length dependent and reaction diffusion control termination in the free radical polymerization of multifunctional (meth)acrylates. *Macromolecules* **2002**, *35*, 7968−7975.

BM025677O